The Thermal Response of Aircraft Cabin Ceiling Materials during a Post-Crash, External Fuel-Spill, Fire Scenario

LEONARD Y. COOPER
Center for Fire Research
National Bureau of Standards
Gaithersburg, Maryland 20899, USA

ABSTRACT

An algorithm is developed to predict the thermal response of aircraft ceiling materials during a post-crash fire scenario. The scenario involves an aircraft's emergency exit doorway which opens onto the flames of a fuel-spill fire which engulfs the fuselage. Data of near-ceiling temperatures acquired during full-scale, post-crash test simulations provide indirect validation of the algorithm. The post-crash time-to-ceiling-ignition is proposed as a measure of cabin fire safety. This measure would be used as a surrogate for the post-crash time available for passengers to safely evacuate the cabin. In this sense, the algorithm is exercised in an example evaluation of the fire safety of a candidate honeycomb ceiling material used together in cabin systems involving polyurethane cushion seating.

INTRODUCTION

The purpose of this investigation is to analyze aircraft cabin ceiling surface temperature data recently acquired during full-scale test simulations of post-crash fires. The analysis is carried out with a view toward the development of a procedure for estimating the temperature histories of overhead aircraft cabin materials subsequent to the ignition of exterior, fuel-spill fires. With such a capability it would be possible to estimate the time for such materials to reach ignition temperatures. This would result in a rational means of ranking the fire safety of candidate overhead aircraft cabin materials.

All tests described here were carried out by the U.S. Department of Transportation Federal Aviation Administration (FAA), Atlantic City, New Jersey.

DESCRIPTION OF THE TESTS

The experiments simulated a wide-body aircraft cabin post-crash fire, similar to those reported previously[1]. The scenario involved a fuselage with two open doorways where one of these is engulfed by an external fuel spill fire. The fire is simulated by a burning 2.44 m x 3.05 m pan of jet fuel (JP-4). The threat to the cabin by this test fire has been shown[1] to be representative of the threat by real, external fuel-spill fires. No-wind conditions were simulated. The test article was a surplus U.S. Air Force C133A cargo aircraft.

The ceiling of the test cabin was made up of 0.0127 m thick rigid Kaowool® ceramic fiber board, where $k = 0.045$ W/mK; $\alpha = 2.67\ (10^{-7})$ m^2/s. A mockup seat made of cushions on a steel frame was placed in the cabin in front of the open doorway exposed to the fire. The study involved eight tests. The only parameter which

varied from test to test was the seat cushion construction. Test 111 is designated as the background test since it involved the seat frame with no cushioning. Data from Test 111 were available for 240 s after ignition. Data from all other tests were only available for 120 s. A schematic of the test setup is presented in Fig. 1.

During the tests, the radiant heat flux near the doorway, and 0.30 m and 0.91 m above the floor, was measured with fluxmeters facing outward toward the fire. Throughout each test, and from one test to another these two fluxes were substantially similar. It will be assumed that this flux, $\dot{q}''_{rad\text{-}door}$, is uniform and isotropic across the entire doorway, and that it can be approximated by the lower flux measured in Test 111 (see Fig. 2).

This study considers near-ceiling temperatures measured by three thermocouples placed in the line traversing the width of the cabin, and directly above the center of the doorway as shown in Fig. 1. The thermocouples were of 24 gage (0.000584 m diameter) chromel/alumel wire. The wire was supported several centimeters from its bead, and there was an attempt to position the bead close to

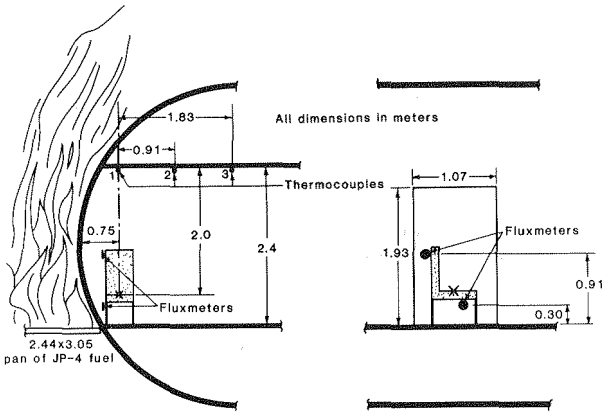

FIGURE 1. A schematic of the test setup.

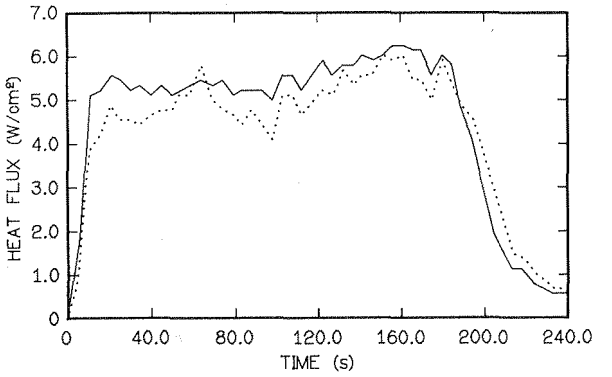

FIGURE 2. Measured doorway heat flux vs time (lower fluxmeter ....; upper fluxmeter ——); test 111 (background).

the ceiling surface so that the bead temperatures would be substantially similar to the nearby, ceiling temperatures. The bead-to-ceiling distances were probably of the order of 0.001 m.

Up to 120 s after ignition, the measured temperatures at each of the three positions and for all eight tests were substantially similar[2]. It is, therefore, reasonable to assume that, for the threat scenario being simulated and up to the 120 s, fire development in a single, mockup seat would not add significantly to the ceiling surface fire threat. Thus, it is assumed to be adequate to study the thermal response of the ceiling only during Test 111. Plots of the measured near-ceiling thermocouple temperatures during this test are presented in Fig. 3.

AN ANALYSIS OF THE THERMAL RESPONSE OF THE CABIN CEILING MATERIAL

Two major phenomena can lead to relatively prompt lower surface heating of the cabin ceiling. The first involves the thick flames and copious products of combustion which engulf the exterior of the fuselage near the exposed, open, doorway. These lead to radiative and convective heat flux to the cabin ceiling.

The convection is from the hot, buoyant gases of the fire which are captured by the open doorway. Upon entering the cabin, these gases are driven upward toward the ceiling, forming an outward (i.e., away from the doorway and toward the cabin interior) moving ceiling jet. After spreading radially from the doorway, this ceiling jet is redirected away from the general location of the doorway and toward the front and rear of the cabin. Eventually the hot, captured, products of combustion start to fill the cabin. They then participate in venting from the second open doorway and in complicated entrainment processes which develop at the fire-exposed, open doorway itself. An analysis of the external fire and the captured flow under rather general wind conditions has been presented previously[3].

The second phenomenon leading to ceiling heating involves the fire which spreads in the seating. Here, the single-seat scenario of the present tests results in only marginally important levels of ceiling heat flux. Yet, fire spread in a fully outfitted cabin could lead to a significant additional threat to the cabin ceiling. The seating fire leads to both radiative and convective heating of the ceiling. The radiation would be primarily from the fire's combustion zone, and the convection from the fire's plume-driven ceiling jet. This ceiling jet would augment the previously mentioned, captured-gas-driven ceiling jet.

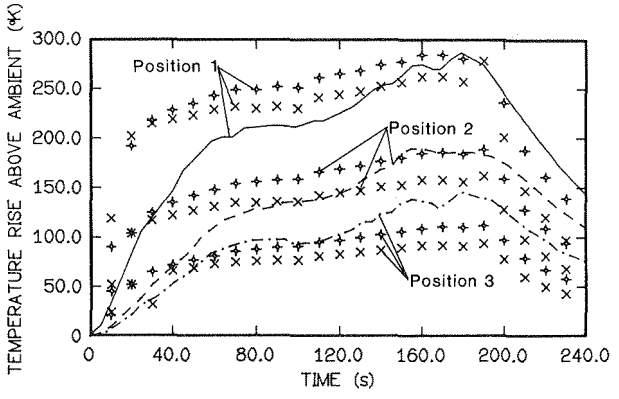

FIGURE 3. Computed Test 111 ceiling temperature (+:β=0.; x:β=3.0 m^2), and corresponding measured near-ceiling temperatures at positions 1, 2, and 3.

Other components of heat flux to/from both the upper and lower ceiling surfaces are radiation from relatively cool, far-field surfaces and reradiation from the ceiling surfaces themselves. In an analysis of the ceiling heating it is reasonable to account for natural convection cooling of the ceiling's upper surface, and to adopt the relatively simple geometry of Fig. 4. Estimates for the components of ceiling heat transfer are developed below. Using these, the problem for the thermal response of the ceiling is then formulated and solved.

Radiation from Doorway to Ceiling

The radiant flux through the door, and to the ceiling is taken to be

$$\dot{q}''_{door\text{-}ceiling} = \dot{q}''_{rad\text{-}door} F_{A\text{-}dA} \qquad (1)$$

where F_{A-dA} is the viewfactor[4] given in Fig. 5.

Captured External Fire Product Gases - An Equivalent Buoyant Source

The "captured gas" doorway plume is modeled by a nonradiating, equivalent, point source of buoyancy located at the center of the horizontal surface of the mockup seat (see Fig. 4). The strength of the equivalent source, $\dot{Q}_{equiv}$, is assumed to be directly proportional to $\dot{q}''_{rad\text{-}door}$. Thus

$$\dot{Q}_{equiv} = \beta \dot{q}''_{rad\text{-}door} \quad (\beta \text{ in } m^2) \qquad (2)$$

Radiation and Convection for the Seating Fire

During the first 120 s of the fire, ceiling heat transfer from the burning single mockup cabin seat was not significant. However, in fully outfitted cabins, it is anticipated that this situation would be changed, especially after the first minute or two subsequent to ignition. By these times, fires in multiple-seat configurations have been observed to grow and spread beyond single seat involvement. Since the present analysis will be extended to fully outfitted cabin scenarios, ceiling heat transfer contributions from the seating fire will be included at the outset.

The seating fire is simulated by a time-dependent point source of energy release rate, $\dot{Q}_{seat}$, assumed to be located with the nonradiating source, $\dot{Q}_{equiv}$, at the center of the horizontal surface of the outer, exposed, doorway seat. A fraction, $\lambda_{r,seat}$, of $\dot{Q}_{seat}$ is assumed to be radiated uniformly over a sphere to the far field. The remaining energy release rate, $(1-\lambda_{r,seat})\dot{Q}_{seat}$, drives the buoyant fire plume upward. Thus, the radiation from the seating fire to the ceiling is assumed to be

$$\dot{q}''_{rad\text{-}seat} = \lambda_{r,seat} \dot{Q}_{seat} / [4\pi H^2 (1 + r^2/H^2)^{3/2}] \qquad (3)$$

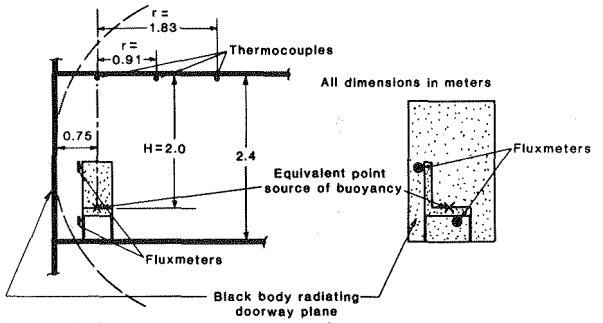

FIGURE 4. A simplified version of the post-crash fire scenario.

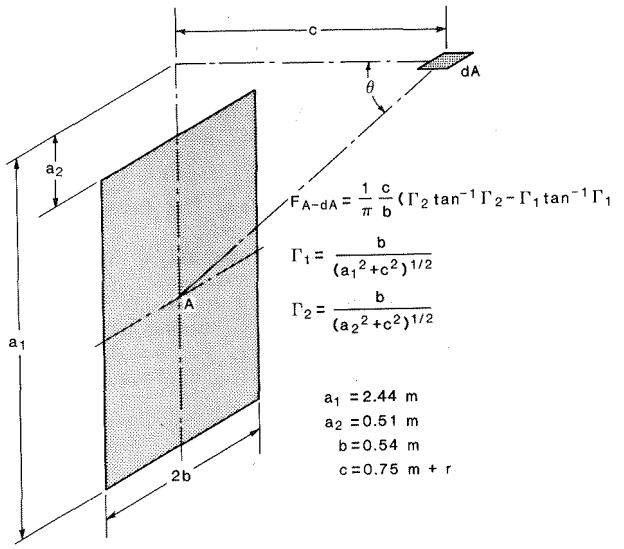

FIGURE 5. The viewfactor between the doorway and a ceiling element.

$\dot{Q}_{seat}$ would vary from one seat cushion construction to another. $\dot{Q}_{seat}$ would typically have to be estimated from test data, and then specified in the present analysis. $\lambda_{r,seat}$ would also vary somewhat from one construction to another, although it is reasonable to choose the value 0.35, a value which characterizes the radiation from flaming combustion zones of many practical fuel assemblies[5]. This value is adopted here.

Convective Heat Transfer from a Combined, Equivalent Source of Buoyancy

$\dot{Q}$, is the combined enthalpy flux of the upward moving combustion gases. Thus

$$\dot{Q}=\dot{Q}_{equiv}+(1-\lambda_{r,seat})\dot{Q}_{seat} \tag{4}$$

All convective heat transfer to the cabin ceiling is from the $\dot{Q}$-generated, plume-driven, ceiling jet, and is estimated by[6,7]

$$\dot{q}''_{conv,L} = h_L\,(T_{ad} - T_{s,L}) \tag{5}$$

$$\frac{(T_{ad}-T_{amb})}{T_{amb}\dot{Q}^{*2/3}} = \begin{cases} 10.22\exp(-1.77r/H), & 0\leq r/H\leq 0.75 \\ 2.10(r/H)^{-0.88}, & 0.75\leq r/H \end{cases} \tag{6}$$

$$h_L/\tilde{h} = \begin{cases} 7.75Re^{-0.5}[1-(5.0-0.390Re^{0.2})(r/H)], & 0\leq r/H\leq 0.2 \\ 0.213Re^{-0.3}(r/H)^{-0.65}, & 0.2\leq r/H\leq 1.03 \\ 0.217Re^{-0.3}(r/H)^{-1.2}, & 1.03\leq r/H \end{cases} \tag{7}$$

$$Q^*=\dot{Q}/(\rho_{amb}C_p T_{amb} g^{1/2}H^{3/2}); \quad \tilde{h}=\rho_{amb}C_p g^{1/2}H^{1/2}\dot{Q}^{*1/3}; \quad Re=g^{1/2}H^{3/2}Q^{*1/3}/\nu \tag{8}$$

The above algorithm is for heat transfer to unconfined ceilings. In using it here, two major assumptions are made; namely, effects of the upper smoke layer are relatively weak during the early times of interest, and the interactions of the ceiling jet and lateral cabin wall surfaces, especially surfaces immediate to the doorway side of the plume-ceiling impingement point, will not lead to total heat transfer flux amplitudes which are significantly larger than peak values that will be estimated with their neglect.

Radiation Between the Lower Ceiling Surface and the Far-Field Cabin Surfaces

The lower ceiling surface is assumed to radiate diffusely to the illuminated surfaces of the cabin and its furnishings. Responding to this, the temperatures of those surfaces also increase with time. However, for times of interest here, it is assumed that these latter temperature increases are always relatively small compared to the characteristic increases of $T_{s,L}$. Accordingly, the net radiation exchange between the ceiling and the nonburning surfaces below can be approximated by

$$\dot{q}''_{rerad,L} = \varepsilon_L \sigma (T^4_{s,L} - T^4_{amb}) \tag{9}$$

Heat Transfer from the Upper Ceiling Surface

Heat is transferred through the ceiling, and eventually the temperature of its upper surface, which is also assumed to be exposed to a constant T_{amb} environment, begins to rise. Heat transfer from this surface has convective and radiative components. These are estimated by

$$\dot{q}''_{conv,U} = h_U (T_{s,U} - T_{amb}); \quad \dot{q}''_{rerad,U} = \varepsilon_U \sigma (T^4_{s,U} - T^4_{amb}) \tag{10}$$

where[8] $h_U = 1.675 |T_{s,U} - T_{amb}|^{1/3}$ W/m^2 (T in K) (11)

The Boundary Value Problem for the Ceiling, and the Method of Its Solution

The temperature field of the ceiling is assumed to be governed by the Fourier heat conduction equation. Initially, the ceiling is at temperature, T_{amb}. The rates of heat transfer to the lower and upper surfaces, are

$$\dot{q}''_L = \dot{q}''_{door-ceiling} + \dot{q}''_{rad-seat} + \dot{q}''_{conv,L} - \dot{q}''_{rerad,L}; \quad \dot{q}''_U = -\dot{q}''_{conv,U} - \dot{q}''_{rerad,U} \tag{12}$$

Radial gradients of variables of the problem are assumed to be small enough so that conduction in the ceiling is quasi-one dimensional in space. An illustration of the idealized, fire scenario is presented in Fig. 6.

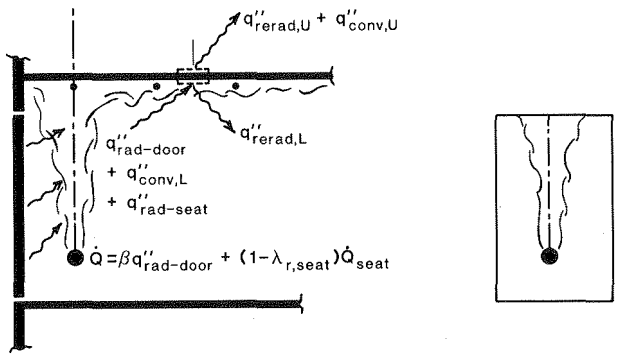

FIGURE 6. The idealized post-crash fire scenario.

A computer program for solving the above problem was developed. The solution to the heat conduction equation for the ceiling at every radial position of interest is by finite differences[10,11]. For a given calculation, $N \leq 20$ equally spaced points are positioned at the surfaces and through the thickness of the ceiling. The spacing of these, δZ, is selected to be large enough to insure stability of the calculation. The change in time for all time steps is made small enough so that, at a given lower surface node, the temperature increases from time step to time step never exceed one percent of the current value of T.

CALCULATION OF THE RESPONSE OF THE CEILING IN THE POST-CRASH TEST SIMULATION

The algorithm was used to predict the response of the Kaowool® ceiling during the first 240 s of Test 111. Here and in the next section all surfaces are assumed to radiate and absorb as black bodies. $\dot{Q}_{seat}$ was taken to zero, and $\dot{q}''_{rad\text{-}door}$ as identical to the Test 111, underseat flux measurement. Ceiling temperatures at positions 1, 2 and 3 were computed for different β's in the range $0 \leq \beta \leq 6.0 m^2$. (This range of β leads to the approximate $\dot{Q}_{equiv}$ range $0 \leq \dot{Q}_{equiv} \leq 300$ kW.) The computed lower ceiling histories for β = 0. and 3.0 m^2 are plotted in Fig. 3.

The Importance of $\dot{Q}_{equiv}$

If convective ceiling heating from doorway-captured products of combustion is equivalent to that from a seat fire of the order of a few hundred kW, then the calculated results plotted in Fig. 3 indicate that such heating is not significant compared to doorway radiation. (Except for the very earliest few seconds, convection from the relatively weak source associated with $\beta=3.0 m^2$ is seen to lead to net cooling of the strongly irradiated ceiling surface.) This result is consistent with earlier observations where variations in single seat cushion construction (peak energy release rates likely never exceeding the few hundred kW level) did not lead to significant differences in near-ceiling temperatures.

Comparisons Between Computed and Measured Temperatures

Per Fig. 3 the peak computed values of ceiling temperature compare favorably with the corresponding peak temperatures measured by the near-ceiling thermocouples. However, the basic qualitative characteristics of the computed and measured transient thermal responses are significanlty different. Namely, the measured temperatures do not have the same type of rapid response which the solution properly predicts for the ceiling surface temperatures. Also, the close tracking of the position 2 and 3 thermocouples at early times does not compare favorably with a like tracking of the computed temperatures.

Two conclusions result from these observations: the thermocouples are not at the temperature of the ceiling surface, and, therefore, data to validate the analysis are not evident. As a result of these conclusions, an analysis of the response of the thermocouples was carried out in order to explain the measured thermocouple responses, and with the hope of obtaining a measure of experimental validation, albeit indirect, for the predicted ceiling response.

AN ANALYSIS OF THE THERMAL RESPONSE OF THE NEAR-CEILING THERMOCOUPLES

The objective of the present analysis is to predict the thermal response of the thermocouples when placed near, but not touching the ceiling. The procedure for positioning these devices prior to testing was such that the thermocouple wires were essentially parallel to the lower ceiling surface and at a distance, d, of the order of 0.001 m. The actual orientation of the wire relative to the doorway plane is unknown. As depicted in Fig. 7, the analysis will consider two extreme configurations for the wire, viz., normal and parallel to the doorway.

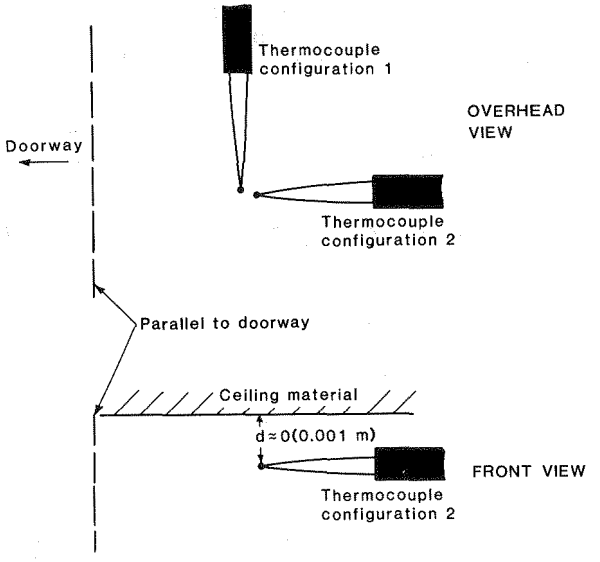

FIGURE 7. Two extreme configurations for placement of the near-ceiling thermocouples.

The characteristic time for conductive heat transfer through the wire thickness is of the order of tenths of a second. It will therefore be assumed that the wire is spatially uniform in temperature. Properties of the chromel/alumel wire will be taken as those of Nickel, viz., ρ=8800kg/m^3, C_p=460Ws/(kgK).

From the literature[5,11,12] it is estimated that the thickness of the ceiling jet within which the thermocouples are submerged are of the order of several centimeters. With a characteristic d, of the order of 0.001 m, it is therefore reasonable to assume that gas velocities local to the thermocouple wire are so small that forced convection vs radiative heating of the wire is negligible. Also, the characteristic Grashof numbers would be relatively small, and any natural convection would be reduced to a conduction limit. This would be dependent on the unknown distance d.

At early times radiation from the doorway drives the temperature increase of the thermocouple. Also, a steady-state analysis which balances doorway heating and radiation exchanges between thermocouple, ceiling and ambient (i.e., which ignores conduction) leads to a result which is consistent with late-time, Fig. 3, measured and computed temperatures of thermocouple and ceiling, respectively.

The thermal analysis which emerges from the above discussion leads to the following equation for the temperature, T_w, of the thermocouple wire

$$\frac{\pi}{4}\rho C_p D^2 \frac{dT_w}{dt} = \dot{Q}'_{door-wire} + \dot{Q}'_{ceiling-wire} + \dot{Q}'_{amb-wire} - \dot{Q}'_{wire} \qquad (13)$$

$$\dot{Q}'_{wire} = \pi D\sigma T_w^4; \quad \dot{Q}'_{amb-wire} = \frac{\pi D}{2}\sigma T_{amb}^4$$

$$\dot{Q}'_{ceiling-wire} = \frac{\pi D}{2}\sigma T_{s,L}^4; \quad \dot{Q}'_{door-wire} = \alpha D \dot{q}''_{door-ceiling} \qquad (14)$$

$$\alpha = \begin{cases} 1 \text{ for configuration 2 of Fig. 7} \\ 1/\sin\theta \text{ (see Fig. 5) for configuration 1 of Fig. 7} \end{cases} \quad (19)$$

To obtain T_w one would specify α and $T_{s,L}$, use the measured values of $\dot{q}''_{rad\text{-}door}$ to obtain $\dot{q}''_{door\text{-}ceiling}$, and solve Eq. (13) subject to $T_w(t=0)=T_{amb}$.

Solutions for T_w in the Test 111 Scenario

The above procedure was applied to the Test 111 scenario. The analysis was carried out numerically for a thermocouple in position 1, 2 or 3 and in configuration 1 or 2. In each case, $T_{s,L}$ was taken from the ceiling temperature calculations described earlier.

T_w calculations were carried out for β values of 2.0 m^2, 3.0 m^2, and 4.0 m^2. β=3.0 m^2 results are presented in Fig. 8, which includes the measured T_w of Fig. 3.

Comparison Between Computed and Measured Temperatures - A Choice for β

Perhaps of greatest significance in Fig. 8 is the early-time thermocouple temperature predictions, which were of particular concern in the ceiling vs thermocouple temperature comparisons of Fig. 3. Here, the simulations of the early, near-linear responses of the thermocouples are noteworthy.

Of further significance is the fact that the calculations reveal a possible explanation for the close tracking of the response of the thermocouples at positions 2 and 3. Namely, such behavior is predicted if the thermocouple wire at position 2 was normal to the door plane (configuration 2), and the thermocouple wire at position 3 was parallel to the door plane (configuration 1).

Fig. 8-type plots provide a basis for selecting the "best" value for β. The β predicting a ceiling response which, in turn, yields the most favorable comparisons between calculated and measured values of T_w would be the obvious choice. Calculations reveal that the T_w predictions are not very sensitive to β variations in the appropriate range 2.0-4.0 m^2. Furthermore, of the values β=2.0 m^2, 3.0 m^2, and 4.0 m^2, all yielded reasonable T_w predictions, and no one of these values clearly yields more favorable T_w predictions than the others. β=3.0 m^2 will be chosen as the "best" value.

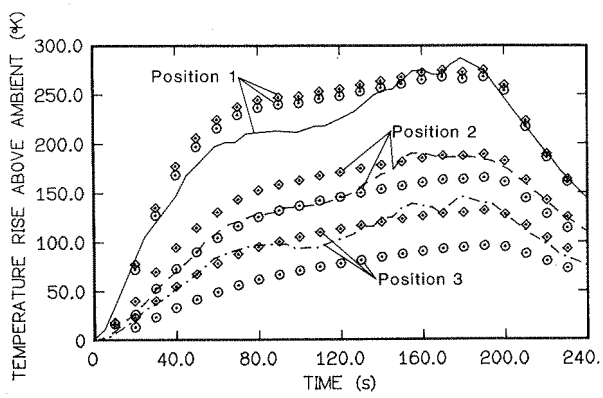

FIGURE 8. Predicted and measured test 111 thermocouple temperatures (β=3.0 m^2). <•>: Predicted T_w, configuration 1; 0: Predicted T_w, configuration 2; ____, __ __ __, __ • __: Measured T_w

PREDICTING THE POST-CRASH TIME-TO-IGNITION OF CEILING CONSTRUCTIONS IN A FULLY SEATED CABIN

The above results provide some confidence in the ceiling thermal response algorithm. To use it to simulate the post-crash fire exposure in a fully-seated cabin, effects of fire spread in an array of seating must be included. This would be done by inputing appropriate, nonzero, $\lambda_{r,seat}$ and $\dot{Q}_{seat}$ terms in Eqns. (3) and (4). Then, using the k and α of a candidate ceiling material, the algorithm would calculate the ceiling's time-dependent, post-crash, thermal response.

In the most likely case of a combustible ceiling material, one could, for example, predict the time for the lower surface to reach a characteristic ignition temperature. Results of a previous FAA program indicate that away from the combustion zone tenable conditions are maintained throughout the cabin prior to ceiling ignition. The time-to-ceiling ignition would therefore provide a reasonable measure of post-crash cabin fire safety, viz., the minimum time available for passengers to evacuate the cabin or the Available Safe Egress Time (ASET)[13]. Hopefully, evaluations of practical cabin ceiling material candidates would lead to associated ignition times, or minimum ASET's, which exceed the time required for cabin evacuation. In any event, the greater the time-to-ignition of a material the better.

In the case of a noncombustible ceiling, time-to-ignition in the above discussion would be replaced by time to reach some agreed upon ceiling temperature, e.g., 600°C, which is often associated with cabin flashover.

Estimates of Post-Crash Fire Growth in Arrays of Cabin Seats - An Example

Estimates of the energy release rate of post-crash fires spreading through arrays of seats were obtained previously[14]. Based on FAA, full-scale, 21 seat tests which were similar to Tests 104-111, estimates of fire growth in two types of seat construction were obtained. The first type of seats, designated as "regular" seats, were made of fire retarded polyurethane foam covered with wool-nylon fabric. The second seat construction was similar to the first, except that it included a blocking layer constructed of a 0.0048 m thick sheet of neoprene with a polyester scrim.

The estimates of $\dot{Q}_{seat}$ for the two types of seats are plotted in Fig. 9. The plots terminate at 140 s and 185 s, at which times video-tape recordings of the tests indicated the initiation of either flashover (140 s) or of rapid development of total obscuration (185 s). These estimates will be used below to evaluate the post-crash response of a specific, honeycomb ceiling material.

POST-CRASH RESPONSE OF A HONEYCOMB CEILING MATERIAL - ESTIMATES OF TIME-TO-IGNITION

The algorithm developed here was used to estimate the post-crash thermal response of a 0.0254 m thick, honeycomb composite, aircraft lining material with an epoxy fiberite covering. The effective thermal properties of the composite were measured, and found to be[15] $k=5.9(10^{-5})$kW/(mK); $\rho=110.$kg/m^3; $\alpha=4.8(10^{-7})$m^2/s; $C_p=1.1$kJ/(kgK). $\dot{Q}_{seat}$ was simulated by the plots of Fig. 9.

The predicted temperature of the ceiling above the doorway seat is plotted in Fig. 10 for both "regular" seating and "blocked" seating. The ignition temperature of the honeycomb material had been measured previously, and was found to be[16] 536°C. Thus, results of Fig. 10 predict onset of ceiling ignition at 148 and 204 s for "regular" and "blocked" seating, respectively. For cabin ceilings of this honeycomb material, blocked rather than unblocked seating would lead to a 56 s advantage in ASET.

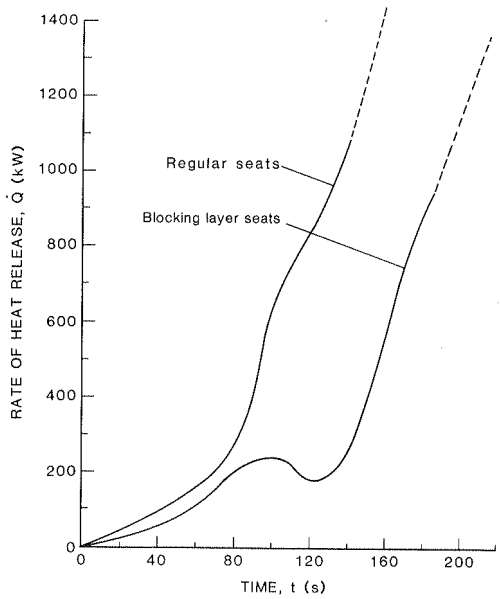

FIGURE 9. Estimate for $\dot{Q}_{seat}$ for arrays of polyurethane seats with and without blocking layers [13] (__ __ __ extrapolated from curves of [13]).

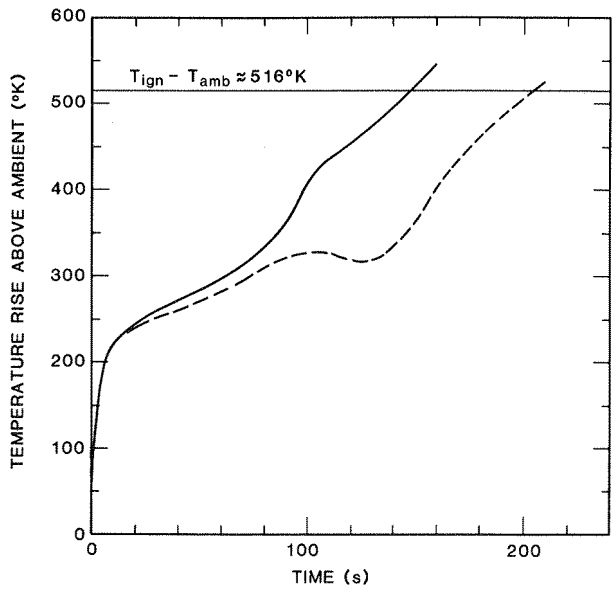

FIGURE 10. Predicated temperature of the honeycomb ceiling material in a cabin with polyurethane seats: with (_____ _____) and without (_____) blocking layers.

REFERENCES

1. Hill, R.G., Johnson, G.R. and Sarkos, C.P., Postcrash Fuel Fire Hazard Measurements in a Wide-Body Aircraft Cabin, FAA-NA-79-42, Fed. Aviation Admin., Atlantic City, NJ, 1979.

2. Cooper, L.Y., The Thermal Response of Aircraft Cabin Ceiling Materials During a Post-Crash External Fuel-Spill Fire Scenario, NBSIR 84-2912, Nat. Bur. of Stand. Gaithersburg, MD, 1984.

3. Emmons, H.W., The Ingestion of Flames and Fire Gases Into a Hole in an Aircraft Cabin for Arbitrary Tilt Angles and Wind Speed, Home Fire Proj. Rpt. 52, Harvard Univ. Div. Appl. Sciences, Cambridge, MA, 1982.

4. Eckert, E.R.G. and Drake, R.M., Heat and Mass Transfer, McGraw-Hill, 1959.

5. Cooper, L.Y., A Mathematical Model for Estimating Available Safe Egress Time in Fires, Fire and Mat., 6, p. 135, 1982.

6. Cooper, L.Y., Heat Transfer from a Buoyant Plume to an Unconfined Ceiling, J. Heat Trans., 104, p. 446, 1982.

7. Cooper, L.Y., Thermal Response of Unconfined Ceilings Above Growing Fires and the Importance of Convective Heat Transfer, 22nd Nat'l. Heat Transfer Conf., ASME Paper 84-HT-105, 1984 and NBSIR 84-2856, Nat. Bur. Stand., Gaithersburg, MD, 1984.

8. Yousef, W.W., Tarasuk, J.D. and McKeen, W.J., Free Convection Heat Transfer from Upward-Facing, Isothermal, Horizontal Surfaces, J. Heat Trans., 104, p. 493, 1982.

9. Emmons, H.W., The Prediction of Fires in Buildings, 17th Symp. (Inter.) on Combustion, p. 1101, 1979.

10. Mitler, H.E. and Emmons, H.W., Documentation for the Fifth Harvard Computer Fire Code, Home Fire Proj. Rpt. 45, Harvard Univ., Cambridge, MA, 1981.

11. Poreh, M., Tsuei, Y.G. and Cermak, J.E., Investigation of a Turbulent Radial Wall Jet, ASME J. of Appl. Mech., p. 457, 1967.

12. Alpert, R.L., Turbulent Ceiling-Jet Induced by Large-Scale Fires, Comb. Sci. and Tech., Vol. 11, p. 197, 1975.

13. Cooper, L.Y., A Concept of Estimating Safe Available Egress Time, Fire Safety Journal, Vol. 5, p. 135, 1983.

14. Steckler, K., Chapter 1: The Role of Aircraft Panel Materials in Cabin Fire and Their Properties, DOT-FAA CT 84/30, Nat. Bur. Stand. rpt. to Fed. Aviation Admin., Atlantic City, NJ, 1985.

15. Parker, W., National Bureau of Standards, private communication.

16. Harkleroad, M., Quintiere, J. and Walton, W., Radiative Ignition and Opposed Flame Spread Measurements on Materials, DOT/FAA/CT-83/28 (Nat. Bur. Stand. rpt. to Fed. Aviation Admin., Atlantic City, NJ, 1983.

NOMENCLATURE

a_1, a_2, b, c	dimensions, Fig. 5
C_p	specific heat
D	wire diameter
d	thermocouple-to-ceiling separation distance
F_{A-dA}	view factor, Eq. (1), Fig. 5
g	acceleration of gravity
H	seat fire-to-ceiling distance
h_L, h_U	lower/upper surface heat transfer coefficient
$\tilde{h}$	characteristic heat transfer coefficient, Eq. (8)
k	thermal conductivity
N	number of grid points in ceiling analysis
$\dot{Q}$, $\dot{Q}^*$	enthalpy flux in plume, Eq. (4), dimensionless $\dot{Q}$, Eq. (8)
$\dot{Q}_{equiv}$, $\dot{Q}_{seat}$	equivalent fire strength, strength of seat fire
$\dot{Q}'_{amb-wire}$, $\dot{Q}'_{ceiling-wire}$	radiation: ambient to wire, ceiling to wire per unit length
$\dot{Q}'_{door-wire}$, $\dot{Q}'_{wire}$	radiation: doorway to wire, from wire per unit length
$\dot{q}''_{conv,U}$, $\dot{q}''_{conv,L}$	convection to upper/lower ceiling
$\dot{q}''_{door-ceiling}$	radiation from doorway to ceiling
$\dot{q}''_{rad-door}$, $\dot{q}''_{rad-seat}$	radiation from doorway, from seat fire to ceiling
$\dot{q}''_{rerad,U}$, $\dot{q}''_{rerad,L}$	radiation from upper/lower ceiling
$\dot{q}''_U$, $\dot{q}''_L$	net heat transfer to upper/lower ceiling
Re	Reynold's number, Eq. (8)
r	distance from plume impingement point
T_{ad}; T_{amb}	adiabatic ceiling temperature, Eq. (6); ambient temperature
$T_{s,U}$, $T_{s,L}$	upper/lower surface ceiling temperature
T_w	thermocouple wire temperature
t	time
Z	indepth ceiling coordinate
α	thermal diffusivity/wire configuration constant, Eq. (15)
β	a constant
Γ_1, Γ_2	constants, Fig. 5
δZ	indepth spacing of ceiling grid points
ε_U, ε_L	lower/upper ceiling emissivity
θ	configuration angle, Fig. 5
$\lambda_{r,seat}$	fraction of $\dot{Q}_{seat}$ radiated
ν	kinematic viscosity of ambient air
ρ, ρ_{amb}	density, density of ambient
σ	Stefan-Boltzmann constant